J Arid Land (2024) 16(1): 46–70
https://doi.org/10.1007/s40333-024-0090-3

Science Press Springer-Verlag

Spatiotemporal changes of gross primary productivity and its response to drought in the Mongolian Plateau under climate change

ZHAO Xuqin[1,2], LUO Min[1,2*], MENG Fanhao[1,2], SA Chula[1,2], BAO Shanhu[1,2], BAO Yuhai[1,2]

[1] College of Geographical Science, Inner Mongolia Normal University, Hohhot 010022, China;
[2] Inner Mongolia Key Laboratory of Remote Sensing and Geographic Information Systems, Hohhot 010022, China

Abstract: Gross primary productivity (GPP) of vegetation is an important constituent of the terrestrial carbon sinks and is significantly influenced by drought. Understanding the impact of droughts on different types of vegetation GPP provides insight into the spatiotemporal variation of terrestrial carbon sinks, aiding efforts to mitigate the detrimental effects of climate change. In this study, we utilized the precipitation and temperature data from the Climatic Research Unit, the standardized precipitation evapotranspiration index (SPEI), the standardized precipitation index (SPI), and the simulated vegetation GPP using the eddy covariance-light use efficiency (EC-LUE) model to analyze the spatiotemporal change of GPP and its response to different drought indices in the Mongolian Plateau during 1982–2018. The main findings indicated that vegetation GPP decreased in 50.53% of the plateau, mainly in its northern and northeastern parts, while it increased in the remaining 49.47% area. Specifically, meadow steppe (78.92%) and deciduous forest (79.46%) witnessed a significant decrease in vegetation GPP, while alpine steppe (75.08%), cropland (76.27%), and sandy vegetation (87.88%) recovered well. Warming aridification areas accounted for 71.39% of the affected areas, while 28.53% of the areas underwent severe aridification, mainly located in the south and central regions. Notably, the warming aridification areas of desert steppe (92.68%) and sandy vegetation (90.24%) were significant. Climate warming was found to amplify the sensitivity of coniferous forest, deciduous forest, meadow steppe, and alpine steppe GPP to drought. Additionally, the drought sensitivity of vegetation GPP in the Mongolian Plateau gradually decreased as altitude increased. The cumulative effect of drought on vegetation GPP persisted for 3.00–8.00 months. The findings of this study will improve the understanding of how drought influences vegetation in arid and semi-arid areas.

Keywords: gross primary productivity (GPP); climate change; warming aridification areas; drought sensitivity; cumulative effect duration (CED); Mongolian Plateau

Citation: ZHAO Xuqin, LUO Min, MENG Fanhao, SA Chula, BAO Shanhu, BAO Yuhai. 2024. Spatiotemporal changes of gross primary productivity and its response to drought in the Mongolian Plateau under climate change. Journal of Arid Land, 16(1): 46–70. https://doi.org/10.1007/s40333-024-0090-3

1 Introduction

With the escalating global warming crisis, mitigation measures such as carbon emission reduction and the promotion of carbon neutrality have attracted worldwide attention, leading to international consensus on the adoption of green and low-carbon strategies (Ji and Lin, 2022; Zhao et al., 2022). Central to these discussions is the role of vegetation gross primary productivity

*Corresponding author: LUO Min (E-mail: luomin@imnu.edu.cn)
Received 2023-07-25; revised 2023-11-10; accepted 2023-11-27

(GPP), which quantifies the amount of organic carbon content captured through photosynthesis in a unit of time. It determines the amount of initial materials and energy that enter the ecosystem (He et al., 2022b). As an important component of the global carbon sink, vegetation GPP profoundly affects the terrestrial carbon cycle.

Long-term and high-precision GPP series are prerequisites for studying the spatiotemporal dynamics and influencing factors of vegetation productivity. Currently, vegetation GPP is mainly estimated through ground surveys, flux observation, remote sensing inversion, and model simulation. Traditional GPP monitoring methods, such as ground survey and flux observation, are primarily based on a sample scale. Due to the strong spatial heterogeneity of GPP, direct GPP observation based on a sample scale cannot reflect the changes in large-scale continuous vegetation productivity; consequently, conducting a comprehensive analysis of the spatiotemporal differentiation and variability characteristics of GPP at a regional scale would be challenging (Piao et al., 2013, 2022). In recent years, remote sensing inversion and model simulation methods have developed rapidly due to their capacity to characterize large-scale vegetation productivity effectively. Hence, they are widely used to calculate regional-scale vegetation productivity (Xiao et al., 2019; Xie and Li, 2020; Chu et al., 2021; Pan et al., 2021). For example, Zhang et al. (2020) used moderate-resolution imaging spectroradiometer (MODIS) GPP to analyze the spatiotemporal distribution and variation characteristics of vegetation GPP in China from 2003 to 2018. The models commonly used for GPP estimation include machine learning models (based on flux tower data), ecosystem process models, and light use efficiency (LUE) models (Jiang and Ryu, 2016; Zhen et al., 2018; Wang et al., 2021b; Guan et al., 2022). Of these, LUE models require only a few input parameters. Moreover, they can directly obtain some key parameters through the inversion of remotely sensed data. These models mainly employ the vegetation index to estimate the photosynthetically active radiation absorbed by the canopy and calculate light energy utilization efficiency, which is the optimal measure of photosynthesis in the vegetation canopy. Therefore, it is widely considered the most effective method to monitor large-scale vegetation productivity and is widely used to study spatiotemporal variation (Vanikiotis et al., 2021; Pei et al., 2022; Xie et al., 2023). For example, Bo et al. (2022) analyzed the spatiotemporal variability and trends concerning GPP in China from 1982 to 2015, primarily relying on the optimum LUE (LUE_{opt}) product.

Additionally, some scholars have further enhanced LUE models by introducing additional factors to improve its accuracy. For instance, Zheng et al. (2020) improved long-term global GPP estimation by adding environmental variables. Yuan et al. (2010) developed the eddy covariance-light use efficiency (EC-LUE) model by substituting the Bowen ratio with the clearness index. This modification not only improved the accuracy of LUE models but also succeeded in developing a series of long-term GPP products. The EC-LUE model can be applied across various types of ecosystems and geographical regions because of its ability to map GPP over extensive areas with high accuracy and applicability while avoiding regional model parameterization (Yuan et al., 2010; Cui et al., 2017; Yu et al., 2018; Wang et al., 2020).

Recent research has highlighted climate change as the primary contributor to vegetation GPP trends in various regions. Wang et al. (2022a) pointed out that changes in water conditions are among the dominant factors determining vegetation carbon sinks. Over the past five decades, global warming in general, coupled with the continuous decrease in precipitation, has led to a marked increase, globally, in the area covered by arid land (Hang et al., 2012; Feng and Fu, 2013), and extreme drought events have become more frequent, bringing unprecedented challenges to the ecosystem. As a crucial factor affecting GPP, drought has gained the attention of scholars (Chen et al., 2021; Xiong et al., 2022). Drought, a natural phenomenon caused by prolonged water scarcity, affects the ecological carbon cycle by altering the underlying physiological processes, such as photosynthesis and respiration (Zhang et al., 2020).

The commonly used drought evaluation indices include the Keetch-Byram drought index (Charlton et al., 2022), standardized precipitation index (SPI) (Hayes et al., 2011), self-calibrating Palmer drought severity index (Huang et al., 2022), and standardized precipitation

evapotranspiration index (SPEI) (Vicente-Serrano et al., 2010a). Focusing on the semi-arid Caucasus Ecoregion, Akhalkatsi (2017) analyzed the factors affecting crop growth and found that seed quality diminishes under soil water stress in arid years, and prolonged drought can lead to crop wilting and death. Wang et al. (2022b) used four different GPP datasets and SPEI data to quantify GPP reductions in global terrestrial ecosystems caused by varying drought severities. The study found that drought-induced GPP reductions intensify with the severity gradient. Additionally, grassland and cropland were found to be the ecosystems most vulnerable to increasing drought severity. Regarding the duration of adverse conditions, even a few months of drought is likely to adversely affect vegetation productivity. Precipitation deficits over a period as short as three months or even shorter could lead to severe drought (Wang et al., 2016). Peng et al. (2019) investigated the cumulative and lagged effects of drought across extra-tropical ecosystems in the northern hemisphere and found 1.00–4.00 accumulated months as a significant duration for the cumulative effect and 2.00–6.00 lagged months for the lagged effect. Many studies have emphasized the importance of considering the cumulative effect duration (CED) when assessing the impact of drought on vegetation GPP, especially in arid and semi-arid regions. For example, Wei et al. (2022) conducted a comparative analysis of the accumulated and lagged effects of drought on global grassland productivity and found the former to be stronger than the latter in most global grasslands. Zhan et al. (2022) employed the multi-scale drought and vegetation index datasets to analyze the impact of drought on vegetation in Yellow River Basin of China, concluding that vegetation areas with low water availability are more susceptible to the cumulative impact of drought. In addition to reduced precipitation, temperature rises significantly contribute to drought. Notably, "hot drought", which occurs when high air temperatures coincide with precipitation deficits, threatens ecosystems as it increases the stress impact caused by greater vapor pressure scarcity. Nevertheless, the extent to which hot and dry atmospheric conditions amplify the impact of inadequate precipitation on the ecological carbon cycle remains unclear (Dannenberg et al., 2022).

The Mongolian Plateau is located in a transitional zone between arid and semi-arid climate zones and is home to various vegetation types that play an important role in the global carbon cycle (Li et al., 2023). In recent decades, warmer and drier climates have caused obvious soil drying and increased degradation of vegetation productivity, threatening the stability of regional ecosystems and the achievements of vegetation construction (He et al., 2022a). However, recent studies concerning the plateau's vegetation GPP have grown in number and achieved valuable results (Chen et al., 2022). Historically, scholars primarily used normalized difference vegetation index (NDVI) to evaluate the vegetation dynamics in this region, focusing on its response to climatic factors such as precipitation and temperature (Guo et al., 2021; Kang et al., 2021; Na et al., 2021). Gu et al. (2022) noted that since 1998, the cumulative effect of drought (7.00–12.00 months) has been the main contributing factor to NDVI as opposed to the lagged effect (10.00–12.00 months). Yin et al. (2023) pointed out that moisture management must be addressed as the main challenge in ecological restoration processes in the Mongolian Plateau. Recently, Meng et al. (2023) identified water availability, temperature, and solar radiation as the most crucial climatic factors contributing to GPP change in 51.21%, 15.51%, and 18.63% of the Mongolian Plateau, respectively. Therefore, it is necessary to analyze the response of vegetation GPP to drought in the Mongolian Plateau.

Against this backdrop, this study aimed to explore the spatiotemporal variability of GPP and its response to different drought indices in the Mongolian Plateau from 1982 to 2018. The impacts of a warming climate on the interaction between vegetation GPP and drought were also revealed. To achieve these objectives, we first identified the spatiotemporal characteristics of changing GPP trends and examined their sustainability using the EC-LUE-generated GPP data. Furthermore, the drought indices (SPEI and SPI) were utilized to analyze the drought trends concerning the Mongolian Plateau over the past 37 years. Finally, the effects of different drought indices on vegetation GPP were determined, and different effects of droughts due to climate warming were also discussed. The novelty of this study lies in the subdivision of the study areas into warming

aridification zones and non-warming aridification zones by analyzing the change in dry and wet trends of the two drought indices (SPEI and SPI) and quantifying the possible effects of temperature rise on the response of GPP to drought. This study provides a scientific basis for comprehensively evaluating the risk of GPP reduction under the single and combined influences of heat stress and drought stress.

2 Study area and data

2.1 Study area

The "Mongolian Plateau" generally refers to the plateau region of Northeast Asia (37°22′–53°23′N, 87°43′–126°04′E), encompassing the entire territories of Mongolia and the Inner Mongolia Autonomous Region of China (hereafter referred to as "Inner Mongolia") (Luo et al., 2021). It extends to the Da Hinggan Ling Mountains in the east, the Altay Mountains in the west, the Sajan and Kente Mountains in the north, and the Yinshan Mountains in the south (Yin et al., 2022). Geographically, the Mongolian Plateau's terrain is elevated in the west and low-lying in the east (Fig. 1a), with an average elevation of 1580 m. The plateau straddles the temperate continental climate zone, receiving an average annual precipitation of about 200 mm; however, it can be higher than 400 mm in the northern and eastern mountainous areas and less than 100 mm in the southwest Gobi desert, as the distance from the ocean increases. Additionally, the temperature in the humid areas of the plateau is lower, while the temperature in the arid areas is higher. The lowest temperature in winter can reach –40°C, and the highest temperature in summer can surpass 35°C (Zhang et al., 2023).

The Mongolian Plateau hosts a complex and diverse range of vegetation. Except in the Gobi desert in the southwest, coniferous forest, deciduous forest, meadow steppe, typical steppe, desert steppe, alpine steppe, shrub, and sandy vegetation are distributed alternately across the plateau (Fig. 1b). Natural grassland, an important component of the temperate grasslands of the northern hemisphere, is the dominant vegetation type in this region. Due to climate change and the resultant decrease in water supply, the Mongolian Plateau often faces droughts of varying severity (Zhang et al., 2022b).

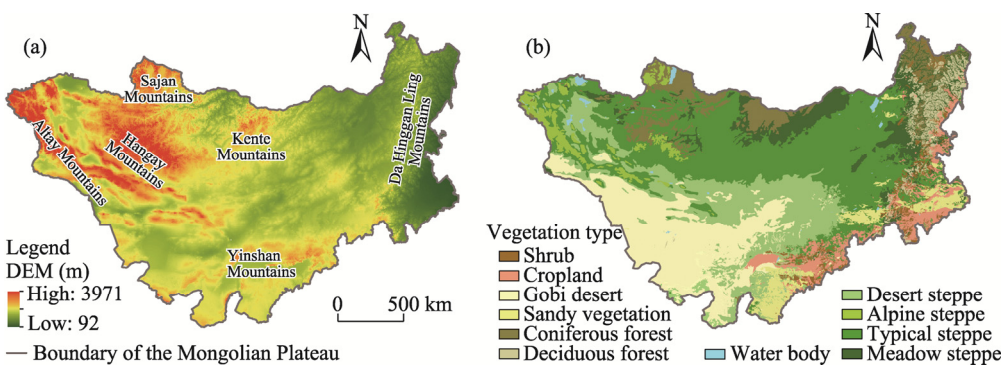

Fig. 1 Digital elevation model (DEM; a) and vegetation type (b) of the Mongolian Plateau

2.2 Data

This study included GPP data from 1982 to 2018, sourced from the National Earth System Science Data Center (http://www.geodata.cn). This data were simulated by the EC-LUE model, with a temporal resolution of 8 d and a spatial resolution of 0.05° (Yuan et al., 2010). The model relied on only four variables: NDVI, photosynthetic active radiation, air temperature, and the Bowen ratio of sensitive to latent heat flux. For this product inspection, the average GPP product of 8 d across all years at 95 sites was extracted. When compared with the measured GPP in the flux sites, the maximum average relative error of GPP was 11.8%. The Global Land Surface Satellite (GLASS) products, characterized by long time series, high resolution, and high precision, offer a reliable

basis for the study of global environmental change. They can be widely used in the global, intercontinental, and regional atmospheres, vegetation cover, and water bodies of dynamic monitoring, and they can be combined with climate change characterization parameters such as temperature and precipitation and applied to the global change analysis. The precipitation and temperature details were obtained from a monthly time series dataset provided by the Climatic Research Unit (CRU) (https://crudata.uea.ac.uk/cru/data/hrg/) of the University of East Anglia, with a spatial resolution of 0.50°. SPEI data were obtained from SPEI base v.2.7 dataset. It was calculated based on the precipitation and potential evapotranspiration data provided by CRU TS 4.05, with a time scale of 1.00–12.00 months and a spatial resolution of 0.50°. The precipitation data from CRU TS 4.05 were further used to derive SPI-related findings. The time scale of SPI is consistent with that of SPEI. The digital elevation model (DEM) data were sourced from the Geospatial Data Cloud (http://www.gscloud.cn). We processed the spatial resolution of the data to 0.50°. The vegetation type map was obtained through the vectorization of 1:1,000,000 vegetation type maps of Inner Mongolia and Mongolia, allowing us to divide the vegetation types in the Mongolian Plateau into nine categories: coniferous forest (7.24%), meadow steppe (8.98%), shrub (2.33%), typical steppe (32.50%), deciduous forest (2.64%), alpine steppe (3.04%), cropland (4.66%), desert steppe (17.12%), and sandy vegetation (3.85%), and two other land use types: water body (0.57%) and Gobi desert (17.07%).

3 Methodologies

3.1 SPI

In this study, we chose two drought indices to investigate GPP response to drought within the context of global warming. SPI, posited by McKee et al. (1993), only considers the influence of precipitation while disregarding the impact of temperature on drought. In 2010, Vicente-Serrano et al. (2010b) proposed the concept of SPEI, which accounts for the evaporation of precipitation due to temperature and thus acknowledges the influence of temperature change on drought. It offers a wider monitoring range for drought compared to SPI. Utilizing these two drought indices not only helps us distinguish the warming aridification and non-warming aridification areas but also quantifies the impact of warming on vegetation's response to droughts.

SPI was calculated using monthly precipitation as the input data. In this study, the gamma distribution probability of precipitation was calculated and then normalized to find the output value of SPI (Neda et al., 2022). Assuming that the precipitation during a certain period is x (higher than zero), the probability density function of the gamma distribution is defined as follows:

$$g(x)=\frac{1}{\beta^{\alpha}\Gamma(\alpha)}x^{\alpha-1}\mathrm{e}^{-\frac{x}{\beta}}, \tag{1}$$

$$\Gamma(\alpha)=\int_0^{\infty}x^{\alpha-1}\mathrm{e}^{-x}\mathrm{d}x, \tag{2}$$

where α (α>0) and β (β>0) are the shape and scale parameters, respectively; $\Gamma(\alpha)$ is the gamma function; and $g(x)$ is the function for calculating the probability density function of the gamma distribution of precipitation.

α and β can be obtained through the maximum likelihood method as follows:

$$\alpha=\frac{1+\sqrt{1+4A/3}}{4A}, \tag{3}$$

$$\beta=\frac{\overline{x}}{\alpha}, \tag{4}$$

$$A=\ln(\overline{x})-\frac{1}{n}\sum_{i=1}^{n}\ln x_i, \tag{5}$$

where A is an intermediate variable; n is the length of the time series (month); $\overline{x}$ is the average value of precipitation at a certain pixel (mm); x_i is the precipitation data series from CRU (mm); and i is the time series. Therefore, the probability of the random variable x being less than the precipitation x_0 in a certain year can be obtained as follows:

$$G(x)=\int_0^x g(x)\mathrm{d}x=\frac{1}{\beta^{\alpha}\Gamma(\alpha)}\int_0^x x^{\alpha-1}\mathrm{e}^{-x/\beta}\mathrm{d}x\,, \tag{6}$$

where $G(x)$ is the cumulative probability for a given time scale.

Suppose that the precipitation during a certain period equals to zero, then the equation would be as follows:

$$H(x)=q+(1-q)G(x)\,, \tag{7}$$

where q is the probability when precipitation equals to zero; and $H(x)$ is transformed into a standard normal variable, which is the value of SPI.

We used SPEI base v.2.7 dataset in this study. SPEI was calculated using precipitation and temperature as input datasets. Potential evapotranspiration calculation requires temperature data, and the difference between precipitation and potential evapotranspiration values was used as SPEI output value. The related calculation process follows the recommendations of Vicente-Serrano et al. (2010a, b):

$$\mathrm{PET}=16F\left(\frac{10T}{I}\right)^{m}\,, \tag{8}$$

$$d'=\left(\frac{T}{5}\right)^{1.514}\,, \tag{9}$$

$$m=6.75\times10^{-7}I^3-7.71\times10^{-5}I^2+1.79\times10^{-2}I+0.492\,, \tag{10}$$

$$F=\left(\frac{N}{12}\right)\left(\frac{\mathrm{NDM}}{30}\right), \tag{11}$$

$$N=\left(\frac{24}{\pi}\right)\arccos\left\{-\tan\varphi\tan\left[0.4093\mathrm{sen}\left(\frac{2\pi J}{365}-1.405\right)\right]\right\}, \tag{12}$$

where PET is the potential evapotranspiration (mm); T is the monthly mean temperature (°C); I is the heat index, calculated as the sum of 12 monthly index values d'; m is the coefficient associated with I; F is the correction coefficient computed as a function of latitude and month; NDM is the number of days in a month (d); N is the maximum number of solar hours (h); φ is the latitude (°); J is the average Julian day of the month (d); and π is the ratio of circumference to diameter.

$$D=\mathrm{PRE}-\mathrm{PET}\,, \tag{13}$$

$$D_z^k=\sum_{i=0}^{k-1}(\mathrm{PRE}_{z-i}-\mathrm{PET}_{z-i}),\ z\geq k\,, \tag{14}$$

where D is the SPEI; PRE is the precipitation (mm); k is the time scale of the aggregation; and z is the calculation number.

3.2 Sen's slope estimation and Mann-Kendall (M-K) test

In this study, Sen's slope estimation and M-K test were used to estimate the changes in vegetation GPP trends and various drought indices. Sen's slope estimation, a nonparametric statistical method, offers high computational efficiency and is insensitive to measurement errors and outliers. It can also effectively reflect the degree to which trends in a certain index over a long duration. Sen's slope (K) is calculated as follows (Agarwal et al., 2021):

$$Q=\frac{Y_{j'}-Y_{i'}}{j'-i'}\,, \tag{15}$$

$$K = \text{median}(Q), \tag{16}$$

where Q is the slope; and $Y_{i'}$ and $Y_{j'}$ are the values of variable Y at times of i' and j', respectively ($1<i'<j'<k$). The median function sorts Q sequence from the smallest value to the largest value. If it is an odd sequence, the median value is taken as K value; and if it is an even sequence, the average of the middle two values is taken as K value.

M-K test can be used to analyze and predict long-term climate series and is often employed to test the significance of changing trends by calculating Sen's slope. M-K test does not require data to follow a normal distribution and remains unaffected by missing values and outliers. Assuming the time series is $\{X_{i'}\}$ (i'=1, 2, ⋯, k) and satisfies the condition $i'\leq j'<k$, the statistics can be calculated as follows (Zhang et al., 2012; Kocsis et al., 2020):

$$S = \sum_{i'=1}^{k-1} \sum_{j'=i'+1}^{k} \text{sgn}(X_{j'} - X_{i'}), \tag{17}$$

$$\text{sgn}(X_{j'} - X_{i'}) = \begin{cases} 1, & (X_{j'} - X_{i'}) > 0 \\ 0, & (X_{j'} - X_{i'}) = 0 \\ -1, & (X_{j'} - X_{i'}) < 0 \end{cases}, \tag{18}$$

$$Z = \begin{cases} \dfrac{S-1}{\sqrt{\text{var}(S)}}, & S > 0 \\ 0, & S = 0 \\ \dfrac{S+1}{\sqrt{\text{var}(S)}}, & S < 0 \end{cases}, \tag{19}$$

where S is the statistic being tested; $X_{j'}$ and $X_{i'}$ are the time series data for variables; Z is the standard normal test statistic, for a given significance level P, and $|Z|>Z_{1-P/2}$ implies that this time series has a significant changing trend at that level; and var(S) is the variance of S, which can be calculated as follows:

$$\text{var}(S) = \frac{k(k-1)(2k+5)}{18}. \tag{20}$$

3.3 Hurst index

Hurst index, based on the analysis method of the rescaled range, is widely used for monitoring the persistence of long-term time series changes (Li et al., 2021). In this study, this method was employed to monitor future continuous changes in vegetation GPP of the Mongolian Plateau. First, we divided the vegetation GPP time series ($\text{GPP}_{(\tau)}$) (τ=1, 2, …, 37) into τ subsequences $\text{GPP}_{(t)}$ (t=1, 2, …, τ). GPP mean time series ($\overline{\text{GPP}_{(\tau)}}$) was then calculated as follows:

$$\overline{\text{GPP}_{(\tau)}} = \frac{1}{\tau}\sum_{t=1}^{\tau} \text{GPP}_{(t)} \ (\tau = 1, 2, \ldots, 37). \tag{21}$$

Subsequently, the cumulative deviation of pixel-by-pixel ($\text{GPP}_{(t,\tau)}$) was calculated using the following equation:

$$\text{GPP}_{(t,\tau)} = \sum_{t=1}^{t} (\text{GPP}_{(t)} - \overline{\text{GPP}_{(\tau)}}), \ (1 \leq t \leq \tau). \tag{22}$$

The range sequence $R_{(\tau)}$ was defined as follows:

$$R_{(\tau)} = \max \text{GPP}_{(t,\tau)} - \min \text{GPP}_{(t,\tau)} \ (\tau = 1, 2, \ldots, 37), \tag{23}$$

where $\text{maxGPP}_{(t,\tau)}$ and $\text{minGPP}_{(t,\tau)}$ (g C/(m^2·a)) are the maximum and minimum values of GPP time series, respectively.

The standard deviation sequence $\text{SD}_{(\tau)}$ was calculated as follows:

$$\mathrm{SD}_{(\tau)}=\left[\frac{1}{\tau}\sum_{t=1}^{\tau}\left(\mathrm{GPP}_{(t)}-\mathrm{GPP}_{(\tau)}^{2}\right)\right]^{1/2}, \tag{24}$$

$$\frac{R_{(\tau)}}{\mathrm{SD}_{(\tau)}}=(\mathrm{c}\tau)^{H}, \tag{25}$$

where c is the constant value; and H is the Hurst index.

Hurst index was obtained using the following equation:

$$\log(R_{(\tau)}/\mathrm{SD}_{(\tau)})_{37}=\mathrm{a}+H\times\log(37), \tag{26}$$

where a is the constant value.

Hurst index has three forms: if Hurst index is equal to 0.5, then time series changes randomly; if Hurst index is greater than 0.5 and less than 1.0, time series has long-term memory, and the future changes would be consistent with past changes; and if Hurst index is greater than 0.0 and less than 0.5, time series would be characterized by anti-persistence; in other words, the future persistent changes would oppose the past change trends (Qu et al., 2020).

According to Sen's slope estimation and Hurst index analysis, we divided the sustainability of GPP changes in the Mongolian Plateau into six scenarios: a non-continuous increase (Hurst index<0.5 and Sen's slope>0.00), a non-continuous decrease (Hurst index<0.5 and Sen's slope<0.00), a continuous non-significant increase (Hurst index>0.5 and Sen's slope>0.00; P>0.05), a continuous non-significant decrease (Hurst index>0.5 and Sen's slope<0.00; P>0.05), a continuous significant increase (Hurst index>0.5 and Sen's slope>0.00; P<0.05), and a continuous significant decrease (Hurst index>0.5 and Sen's slope<0.00; P<0.05).

3.4 Division of warming aridification areas

Furthermore, in order to identify the contribution of temperature rise to drought, we divided the Mongolian Plateau into warming aridification areas and non-warming aridification areas based on the dry and wet change trends of SPI and SPEI. The criteria employed in this study were as follows: the areas indicated as not significantly drying when SPI was used but significantly drying when SPEI was used were identified as areas with mild aridification due to climate warming; the areas indicated as wetting when SPI was used but not significantly drying when SPEI was used were identified as areas with moderate aridification; and the areas indicated as wetting when SPI was used and significantly drying when SPEI was used were identified as areas with severe aridification (Zhang et al., 2022a).

3.5 Correlation analysis and regression analysis

In this study, the influence of temperature and drought indices on GPP was judged by correlation analysis and multiple correlation analysis. The correlation coefficient can represent the impact extent of climate factors on GPP, and the multiple correlation coefficient reflects the comprehensive influence of multiple independent variables on one dependent variable.

Taking temperature as an example, the correlation coefficient (R_{UV}) between GPP and temperature can be calculated using the following formula (Wu et al., 2022):

$$R_{UV}=\frac{\sum_{i'=1}^{k}(U_{i'}-\bar{U})(V_{i'}-\bar{V})}{\sqrt{\sum_{i'=1}^{k}(U_{i'}-\bar{U})^{2}}\sqrt{\sum_{i'=1}^{k}(V_{i'}-\bar{V})^{2}}}, \tag{27}$$

where $\bar{U}$ and $\bar{V}$ are the average values of GPP (g C/m^2) and temperature (°C), respectively; and $U_{i'}$ and $V_{i'}$ are the values of GPP (g C/m^2) and temperature (°C) at time i', respectively. The value range of R_{UV} is [–1, 1]. The larger the absolute value of R_{UV}, the greater the influence of temperature on GPP.

We used the multiple correlation coefficient to identify the degree of influence of drought indices (SPI and SPEI) and temperature on GPP. The multiple correlation coefficient ($r_{u,vw}$) can be calculated as follows:

$$r_{u,vw} = \sqrt{1-(1-r_{uv}^2)(1-r_{uw,v}^2)}\,, \tag{28}$$

where r_{uv} is the correlation between GPP and drought indices; and $r_{uw,v}$ is the partial correlation coefficient between GPP and drought index (SPI or SPEI) after the temperature is fixed.

The regression coefficients can be used to compare and analyze the sensitivity of vegetation GPP to different climatic factors. Since the dimensions of the indicators are not uniform, they must be normalized using the following equation before regression analysis (Wang et al., 2018):

$$Z(E) = \frac{E-\overline{E}}{S(E)}\,, \tag{29}$$

where $Z(E)$ is the standardized time series; E is the GPP, SPI, SPEI, or temperature series; $\overline{E}$ is the average value of each series; and $S(E)$ is the standard deviation of the corresponding series. The regression equation was then established, as follows, for the standardized parameters:

$$y_i = a_i x'_{iT} + b_i x'_{iS} + \varepsilon_i\,, \tag{30}$$

where y_i is the normalized GPP series; x'_{iT} is the normalized temperature series; x'_{iS} represents the normalized drought indices; ε_i is the residual error; and a_i and b_i are the regression coefficients of temperature and drought indices, respectively. The values of a_i and b_i reflect the sensitivity of GPP to temperature and drought indices.

In this study, we used "*t*-test" to determine the significance of the regression coefficient to ascertain whether the effect of the independent variables on the dependent variable was significant. The ratio of the regression coefficient and the standard error of the regression coefficient were used as *t*-values. Generally, $P<0.05$ represents a significant effect on GPP (Xu et al., 2003).

3.6 Calculating CED

CED refers to the cumulative effect of drought on vegetation on a continuous time scale. The correlation coefficient is calculated for monthly GPP values and drought indices over 1.00–12.00 months. The cumulative month, where the maximum correlation coefficient is located, represents the cumulative effect of drought on vegetation GPP (Wei et al., 2022) as seen in the following two equations:

$$r_l = \mathrm{corr}(\mathrm{GPP},\ AI_l)\ (1.00 \le l \le 12.00)\,, \tag{31}$$

$$r_{\max-\mathrm{cum}} = \max(r_l)\ (1.00 \le l \le 12.00)\,, \tag{32}$$

where r_l is the correlation coefficient between GPP and drought indices; l is the monthly cumulative drought indices for 1.00–12.00 months; AI is the drought indices; and $r_{\max-\mathrm{cum}}$ is the maximum correlation between GPP and drought indices.

4 Results

4.1 Trends in GPP and drought indices changes in the Mongolian Plateau

Between 1982 and 2018, the changing rate of vegetation GPP in the Mongolian Plateau ranged from –10.64 to 12.42 g C/(m^2·a), and the spatial heterogeneity in these trends was significant (Fig. 2a). Vegetation GPP increased in 49.47% of the plateau's total vegetation-covered area (18.37% of which showed a significant increase), concentrated in the southeast and northwest regions of the Mongolian Plateau. Meanwhile, the areas with significant and non-significant downward trends in GPP accounted for 10.77% and 39.76%, respectively, primarily distributed along northern Mongolia and northeastern and central Inner Mongolia (Fig. 2b). Regarding the different vegetation types, the most notable GPP increase was observed in the restoration of sandy vegetation, with 66.09% of areas indicating a significant upward trend. It was followed by cropland and shrub, with 54.41% and 45.51% of the land, respectively, exhibiting an upward trend in GPP. In contrast, meadow steppe and deciduous forest experienced considerable degradation, with over 80.00% of these areas indicating a downward trend in GPP (Fig. 2c).

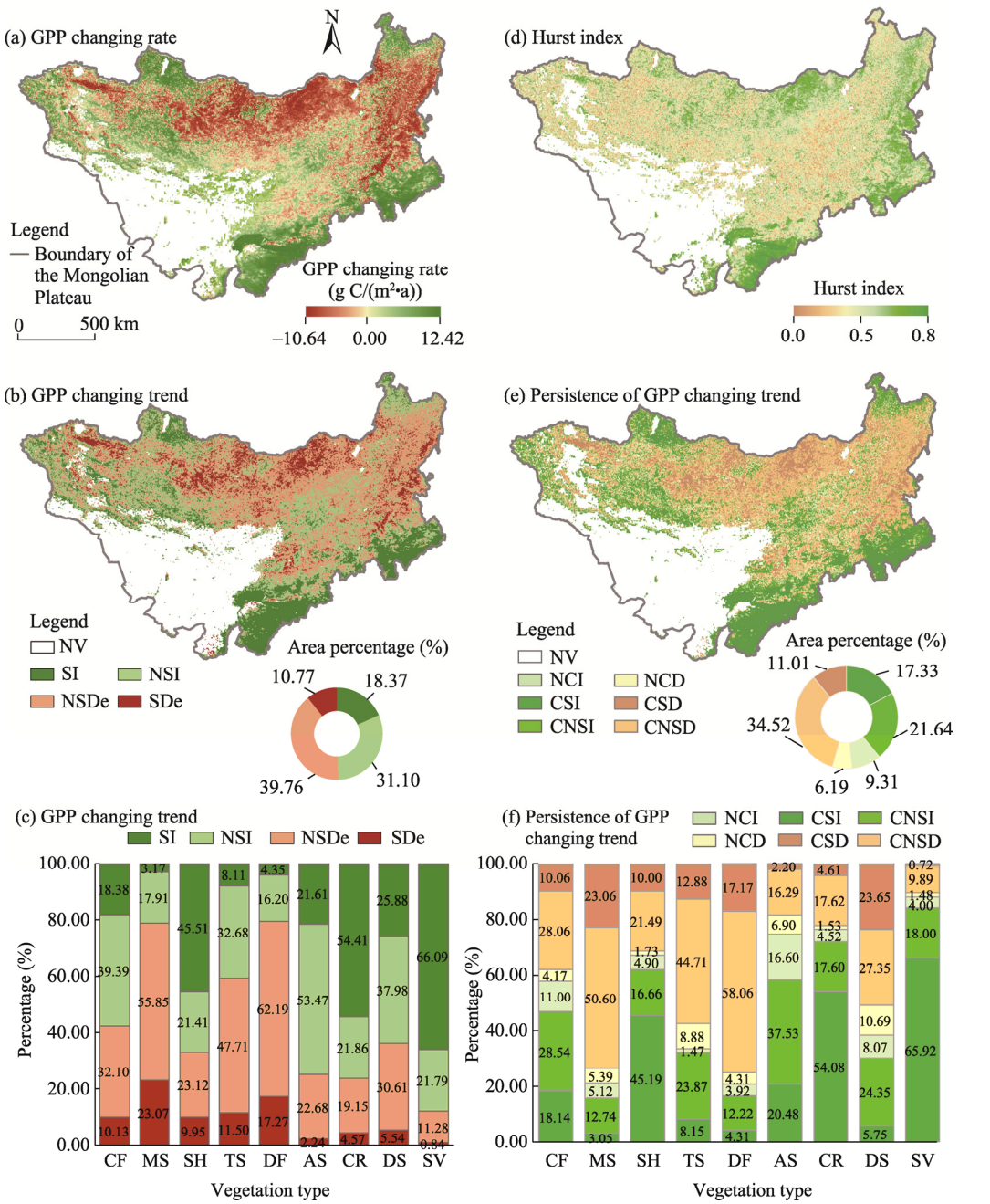

Fig. 2 Trends in gross primary productivity (GPP) changes and their persistence in the Mongolian Plateau. (a), spatial distribution of GPP changing rate; (b), classification of the significance of GPP changing trends; (c), GPP changing trends in different vegetation types; (d), spatial distribution of Hurst index; (e), persistence of GPP changing trends; (f), persistence of GPP changing trends in different vegetation types. NV, non-vegetation area; SI, significant increase; SDe, significant decrease; NSI, no significant increase; NSDe, no significant decrease; NCI, non-continuous increase; NCD, non-continuous decrease; CSI, continued significant increase; CSD, continued significant decrease; CNSI, continued non-significant increase; CNSD, continued non-significant decrease; CF, coniferous forest; MS, meadow steppe; SH, shrub; TS, typical steppe; DF, deciduous forest; AS, alpine steppe; CR, cropland; DS, desert steppe; SV, sandy vegetation.

Combined with the results of Hurst index analysis, we also examined the sustainability of GPP trends in the Mongolian Plateau. GPP changes in 84.50% of the Mongolian Plateau showed a continuous and stable trend (Hurst index>0.5), of which 38.97% displayed a continuous upward

trend in GPP, mainly in the northern and southeastern parts of the plateau. In contrast, a continuous downward trend was mainly observed in the central part of the Mongolian Plateau (45.53%), suggesting a more promising outlook for vegetation changes in the southeast, northwest, and northeast marginal areas of the Mongolian Plateau than in the middle part. Areas of unstable changes were only noted in 15.50% of the total vegetation-covered area (Fig. 2d and e). Significant differences were observed in the persisting trends of GPP changes among different vegetation types. GPP of shrub, cropland, and sandy vegetation increased continuously (these areas had a continuous upward trend, accounting for more than 60.00% of these areas), while GPP of meadow steppe and deciduous forest decreased significantly (showing a continuous downward trend, accounting for more than 70.00% of these areas; Fig. 2f).

The changes in SPI and SPEI in the Mongolian Plateau from 1982 to 2018 displayed strong spatial heterogeneity (Fig. 3). Since SPEI considers the effects of both precipitation and temperature changes, the drought area monitored using SPEI is wider than that monitored using SPI. Based on the results of changes concerning SPI, the area of the Mongolian Plateau indicating a drying trend accounted for 30.12% (Fig. 3b), which was far lower than the dried area monitored using SPEI (92.27%; Fig. 3e). This indicates an undeniable drying trend in the plateau caused by rising temperatures over the past 37 years. The drought-stricken areas of the Mongolian Plateau that were monitored using SPI were primarily concentrated in the Altay Mountains in the west, the Da Hinggan Ling Mountains in the east, and the Kente Mountains in the central region. SPI-based monitoring revealed that 69.88% of the Mongolian Plateau displayed a wetting trend (with 5.82% passing the significance test), mainly located in the southwest region (Fig. 3a and b). However, about 92.27% of the Mongolian Plateau showed a drying trend as per SPEI. Of these areas, 36.10% were identified as significantly drying, mainly located in the central and southern parts of the plateau. Only 7.73% of the areas exhibited an insignificant wetting trend; these areas were sporadically distributed in the eastern and northwestern mountainous areas (Fig. 3d and e). Significant discrepancies were evident in the findings after comparing SPI and SPEI assessments across different vegetation areas. SPI results indicated that typical steppe, desert steppe, cropland, and sandy vegetation areas were mainly wetting, while deciduous forest areas were drying in a large area (87.50%), indicating reduced precipitation in this area (Fig. 3c). According to SPEI-referenced findings, all the different vegetation types were mainly drying, especially in desert steppe (73.17%; Fig. 3f).

By further dividing the observed drying and wetting trends associated with different drought indices, 71.39% of the Mongolian Plateau was found to be affected by varying severity of drought caused due to the rise in temperatures (Fig. 4). Of this area, 35.30% constituted moderate warming aridification areas, mainly concentrated in the Hangay Mountains in northern Mongolia, in western Inner Mongolia, and toward the south of the Da Hinggan Ling Mountains. The mild warming aridification areas closely corresponded to those areas indicated as not significantly dry based on SPI. Southern Mongolia and the central and western parts of Inner Mongolia were categorized as severe warming aridification areas, accounting for 28.53% of the entire plateau (Fig. 4a). Notably, desert steppe and sandy vegetation exhibited aridification due to warming, affecting 92.68% and 90.24% of the areas, respectively. Also, the severe warming aridification area in desert steppe accounted for more than half of its total land area (54.15%). Moderate and severe warming aridification areas accounted for 65.85% and 24.39% of sandy vegetation, respectively. Additionally, the arid areas of cropland and typical steppe accounted for more than 50.00% of their territories, indicating that temperature rise greatly increases the drought stress of these vegetation types. In contrast, deciduous forest displayed the least sensitivity to temperature rise, with arid areas accounting for only 12.50% of their total area (Fig. 4b).

4.2 Correlation analysis of GPP with temperature and drought indices

The spatial distribution of correlation between different drought indices (SPI and SPEI) and GPP in the study area was similar, with primarily positive correlations (Fig. 5). The positive

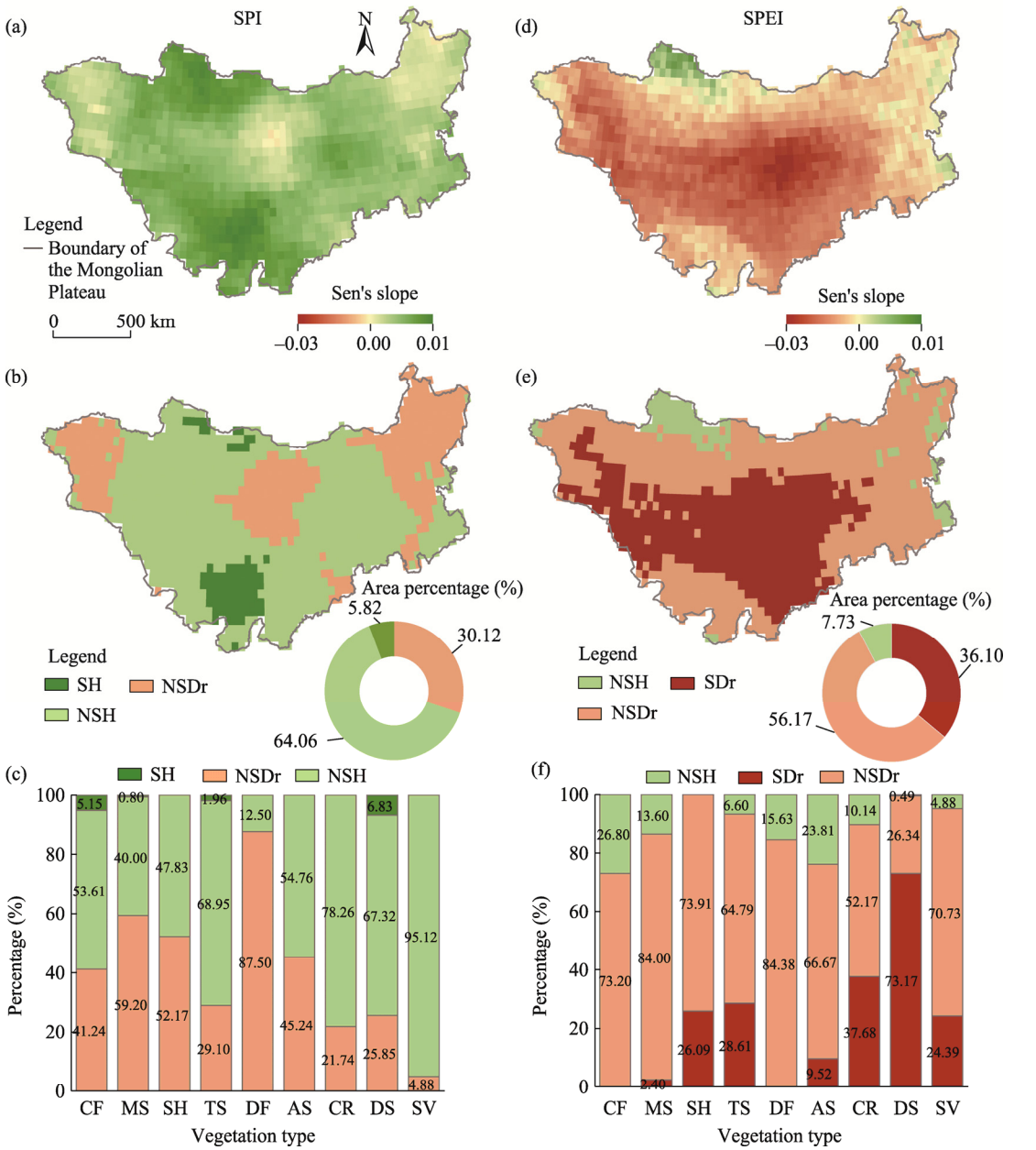

Fig. 3 Variation trends of drought indices in the Mongolian Plateau. (a), spatial distribution of Sen's slope of the standardized precipitation index (SPI); (b), classification of changing trends of SPI; (c), SPI changes in different vegetation types; (d), spatial distribution of Sen's slope of the standardized precipitation evapotranspiration index (SPEI); (e), classification of changing trends of SPEI; (f), SPEI changes in different vegetation types. SH, significant humidification; SDr, significant dryness; NSH, non-significant humidification; NSDr, non-significant dryness.

correlations of SPI and SPEI with GPP accounted for 89.66% and 81.98% of the total vegetation-covered area, respectively. Furthermore, significant positive correlations constituted 31.71% and 21.45%, respectively, mainly concentrated in the eastern Mongolian Plateau. These results suggest that the vegetation in these areas is affected by moisture conditions. The areas where GPP exhibited negative correlations with SPI and SPEI were mainly distributed in the northwest, the eastern mountainous areas, and parts of the southwest, accounting for 10.33% and 18.02% of the total vegetation-covered area, respectively. Most of these areas were not significant (Fig. 5a, b, d,

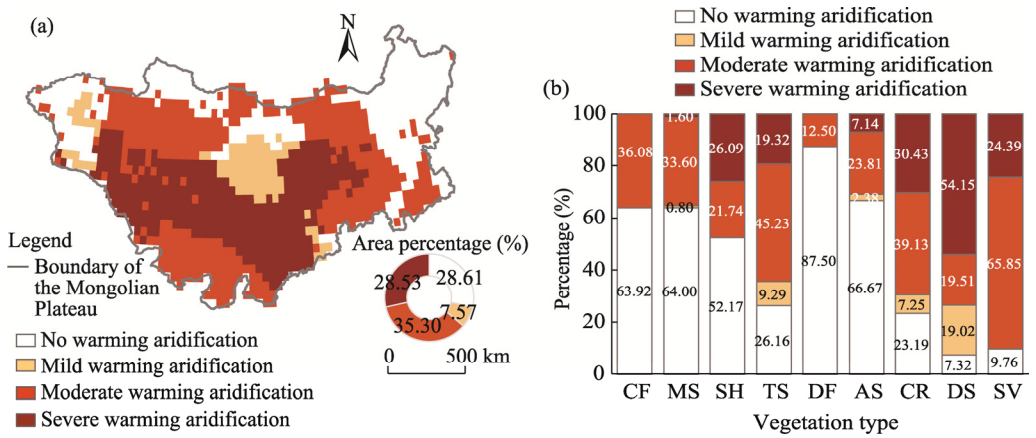

Fig. 4 Spatial distribution of warming aridification areas in the Mongolian Plateau (a) and the percentage of warming aridification areas in different vegetation types (b)

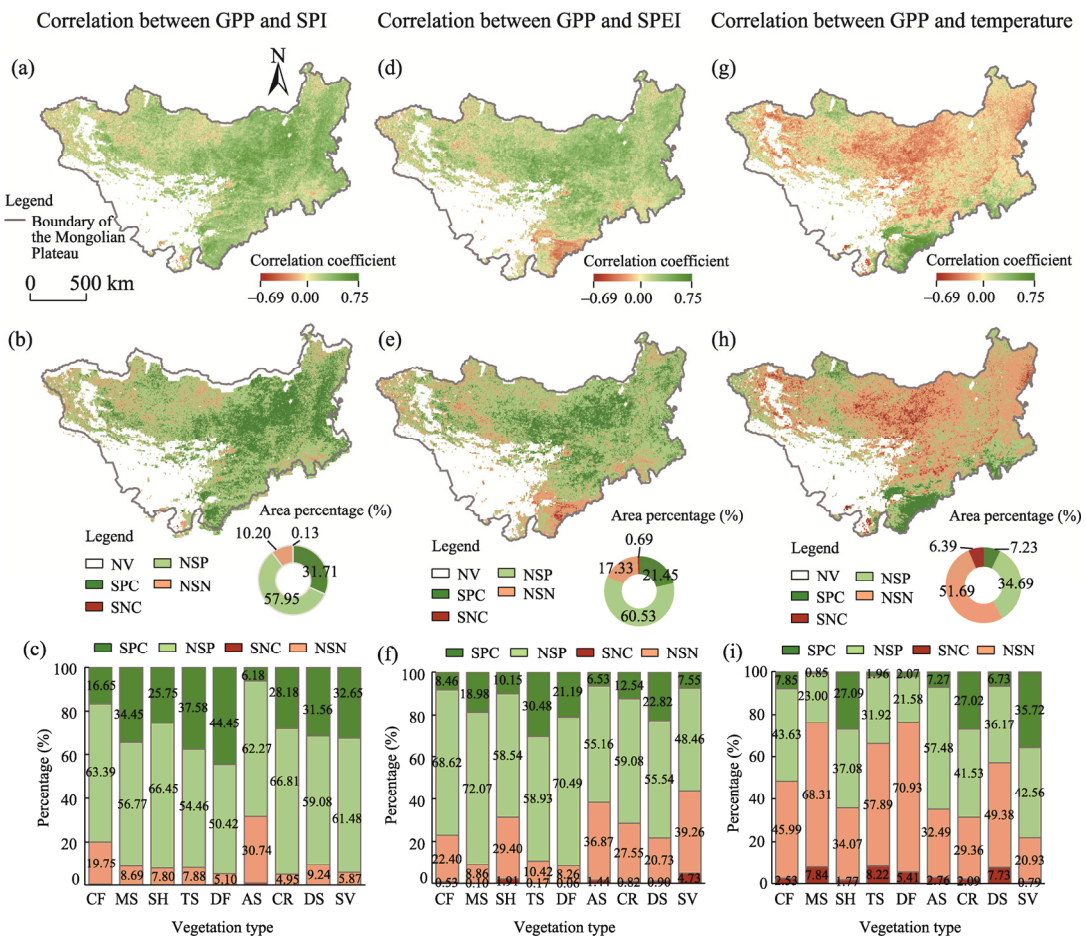

Fig. 5 Spatial distribution and classification of correlation coefficients between GPP and SPI (a and b), GPP and SPEI (d and e), and GPP and temperature (g and h), and the percentage of the classification of correlation coefficients in different vegetation types (c, f, and i). SPC, significantly positive correlation; SNC, significantly negative correlation; NSP, non-significantly positive correlation; NSN, non-significantly negative correlation.

and e). Meanwhile, GPP in these areas was mainly positively correlated with temperature, possibly due to the relatively high altitude, abundant moisture conditions, and low temperature of these

areas. Furthermore, the carbon sequestration of vegetation is mainly limited by thermal conditions. Additionally, a negative correlation was observed between temperature and GPP in other areas of the Mongolian Plateau (58.08%; Fig. 5g and h), indicating that increased temperatures did not correspond to an increase in the carbon sequestration capacity of local vegetation.

GPP and drought indices of different vegetation types exhibited predominantly positive correlations (56.00%–95.00%). The positive correlation between GPP and SPI of cropland and deciduous forest was higher, accounting for more than 94.00% of the areas (Fig. 5c). The area with a positive correlation between GPP and SPI was larger than the area with a positive correlation between GPP and SPEI for various vegetation types (Fig. 5f). The statistical results regarding the correlation between GPP and temperature showed that GPP trends in meadow steppe, typical steppe, and desert steppe were in contrast to the changing trend of temperature. Consequently, an increase in temperature would negatively impact the growth of such vegetation. However, 78.28% of sandy vegetation GPP was positively correlated with temperature, indicating that temperature rise promotes GPP synthesis in sandy vegetation (Fig. 5i).

The multiple correlation distributions of GPP with temperature and the two drought indices were relatively consistent (Fig. 6). The multiple correlation coefficients of GPP with SPI, SPEI, and temperature ranged from 0.00 to 0.81. The areas significantly affected by temperature and drought as per SPI accounted for 27.65% of the total vegetation-covered area, primarily distributed in the central, eastern, and southeastern parts of the Mongolian Plateau (Fig. 6b). In contrast, the area significantly correlated with temperature and SPEI showed a decrease. The decrease in significantly related areas was mainly concentrated in the Da Hinggan Ling Mountains (Fig. 6e). Notably, the multiple correlations among shrub, cropland, and sandy vegetation were significant, indicating that the combined action of temperature and drought has a stronger impact on GPP of these vegetation types (Fig. 6c and f).

4.3 Sensitivity of GPP to drought and temperature

An analysis of the sensitivity of GPP to drought indices and temperature from 1982 to 2018 revealed that GPP in the Mongolian Plateau was more sensitive to drought than to temperature, especially in the central and eastern parts (Fig. 7). The regression coefficients of GPP with SPI, SPEI, and temperature ranged from –0.85 to 1.00 (Fig. 7a, b, e, and f). Overall, 65.20% (63.12%) of vegetation GPP in the Mongolian Plateau was found to be primarily and positively controlled by SPI (SPEI). Based on SPI and SPEI, the areas where GPP was primarily influenced by temperature accounted for 34.80% and 36.88% of the vegetation-covered area, respectively. The areas where temperature emerged as the most important limiting factor were similar, with SPI and SPEI as control, and were concentrated in the northwestern mountainous region and the southeastern region (Fig. 7c and g). The heightened positive sensitivity of GPP to drought, with SPEI and temperature as independent variables, was more pronounced than the correlation observed with SPI as independent variables (Fig. 7a and b). Since only the effect of precipitation is considered when SPI is the independent variable, while SPEI considers not only the effect of precipitation but also the effect of temperature, this suggests that the effect of temperature on drought increases the response of vegetation to drought sensitivity. Furthermore, the sensitivity of GPP to temperature and drought exhibited notable differences among various vegetation types. GPP of meadow steppe, typical steppe, deciduous forest, and desert steppe was found to be more sensitive to drought than to temperature, and the areas where drought was the primary control accounted for more than 60.00% (Fig. 7d and h).

To determine the impact of warming on vegetation's response to drought, we calculated the sensitivity differences of GPP to drought in warming aridification areas and non-warming aridification areas across various vegetation types. The results indicate an alteration in the sensitivity of GPP to drought in various vegetation types due to rising temperatures (Fig. 8). Except for deciduous forest and sandy vegetation, the response of GPP to SPI increased with rising temperatures. Meanwhile, the response of coniferous forest, meadow steppe, deciduous

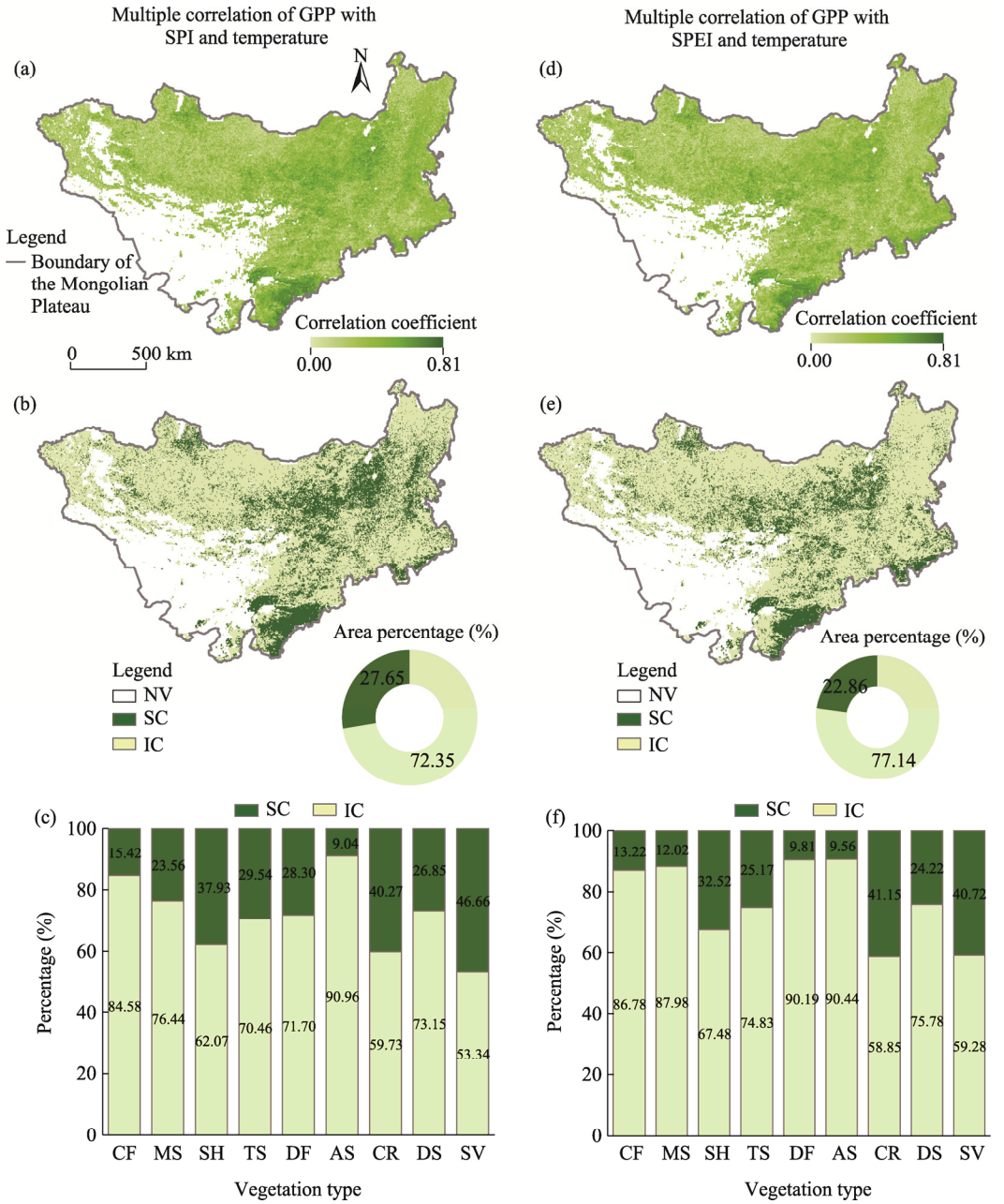

Fig. 6 Spatial distribution and classification of multiple correlation coefficients of GPP with SPI and temperature (a and b), and GPP with SPEI and temperature (d and e), and the percentage of the classification of multiple correlation coefficients in different vegetation types (c and f). SC, significant correlation; IC, insignificant correlation.

forest, and alpine steppe to SPEI was aggravated, and the sensitivity of typical steppe, cropland, desert steppe, and sandy vegetation to SPEI was weakened. The difference in the sensitivity of GPP to drought between warming aridification areas and non-warming aridification areas of sandy vegetation was –0.24, which was considerably greater than that of other vegetation types.

4.4 CED of drought on vegetation GPP

Regarding SPI, the average CED of drought on vegetation GPP was about 5.77 months, with durations exceeding 10.00 months in the northeastern, southern, and central parts of the Mongolian Plateau (Fig. 9a). The average CED according to SPEI was 5.90 months. Overall,

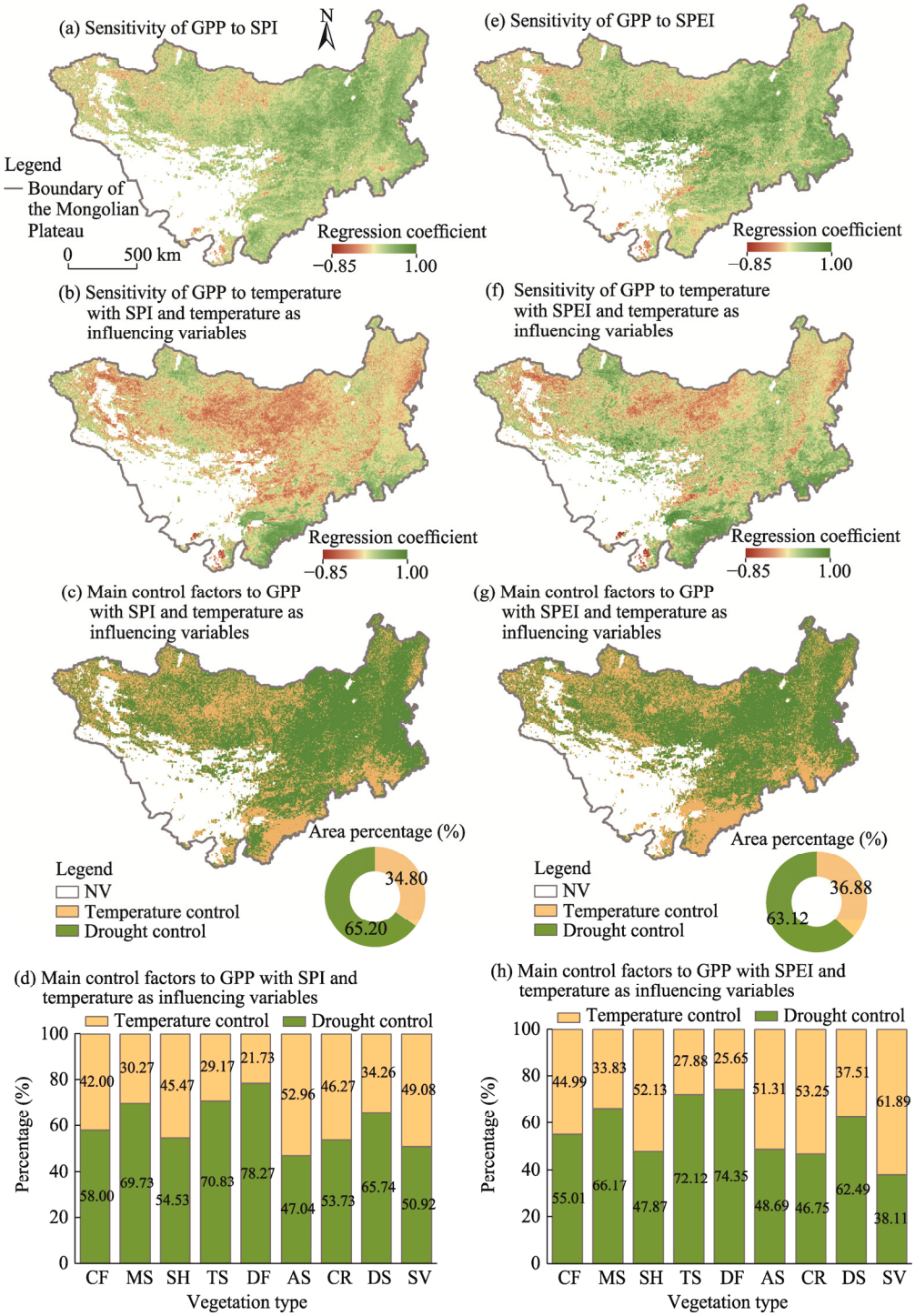

Fig. 7 Sensitivity of GPP to drought indices and temperature and spatial distribution of main control factors. (a), spatial distribution of the sensitivity of GPP to SPI; (b), spatial distribution of the sensitivity of GPP to temperature with SPI and temperature as influencing variables; (c), spatial distribution of main control factors to GPP with SPI and temperature as influencing variables; (d), the percentage of main control factors to GPP in different vegetation types with SPI and temperature as influencing variables; (e), spatial distribution of the sensitivity of GPP to SPEI; (f), spatial distribution of the sensitivity of GPP to temperature with SPEI and temperature as influencing variables; (g), spatial distribution of main control factors to GPP with SPEI and temperature as influencing variables; (h), the percentage of main control factors to GPP in different vegetation types with SPEI and temperature as influencing variables.

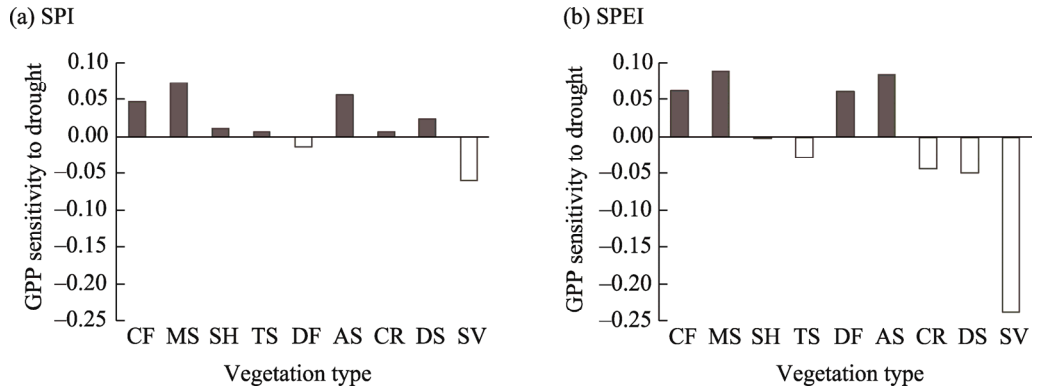

Fig. 8 Effects of temperature rise on the sensitivity of GPP to drought in different vegetation types. (a), SPI; (b), SPEI.

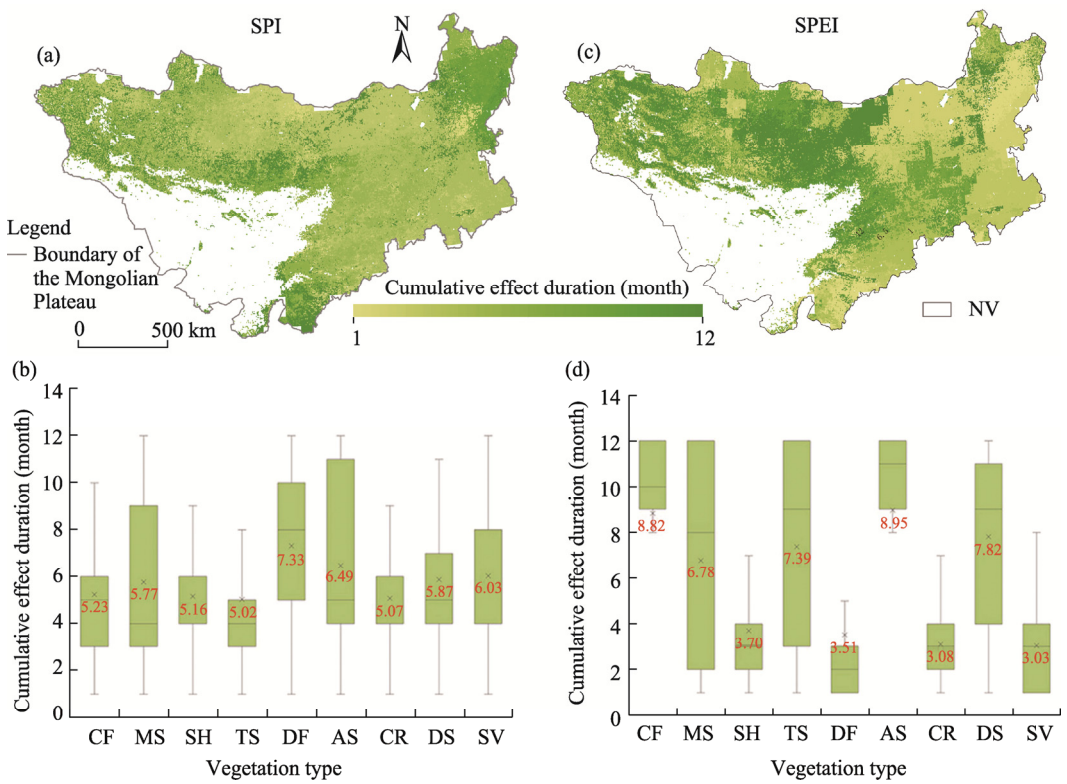

Fig. 9 Spatial distribution of cumulative effect duration of drought obtained using SPI (a) and SPEI (c), and variation of cumulative effect duration of drought obtained using SPI (a) and SPEI (c) for different vegetation types. The boxes represent the range from the lower quantile (Q25) to the upper quantile (Q75). The cross symbols and horizontal lines inside the boxes represent the means and medians, respectively. The upper and lower whiskers indicate the maximum and minimum values, respectively.

CED of SPEI on vegetation GPP in the eastern region was longer than that in the northwestern region, indicating greater drought resilience in the eastern region (Fig. 9c). Based on SPI, the average CED of different vegetation types ranged from 5.02 to 7.33 months, with CED of deciduous forest and alpine steppe reaching 7.33 and 6.49 months, respectively; CED of other vegetation types remained concentrated around 5.00–6.00 months (Fig. 9b). Based on SPEI, the average CED for different vegetation types ranged from 3.03 to 8.95 months, with significant among different vegetation types. Coniferous forest, meadow steppe, typical steppe, alpine steppe, and desert steppe displayed relatively long CED, ranging from 6.78 to 8.95 months. In contrast, the drought resistance of shrub, deciduous forest, cropland, and sandy vegetation in the

Mongolian Plateau was relatively similar, with CED lasting for 3.00–4.00 months, which was comparable to SPEI (Fig. 9d). These observations imply that CED is closely associated with the differences in various vegetation conditions and the external environment.

5 Discussion

5.1 Sensitivity of vegetation GPP to drought

The analysis of the temporal variation characteristics of vegetation GPP in the Mongolian Plateau from 1982 to 2018 reveals that the vegetation in the northwest and southeast regions of the plateau has recovered well over these 37 years, corroborating with previous findings (Meng et al., 2023). This recovery shows the effectiveness and significance of the implemented ecological projects, such as sandstorm control and farmland-to-forest restoration. The results show that the drought severity in the Mongolian Plateau has significantly increased over the past 37 years as a result of rising temperatures, especially in typical steppe, cropland, desert steppe, and sandy vegetation areas. Considering that transpiration and evaporation consume around 80.00% of precipitation (Abramopoulos et al., 1988), SPEI is more suitable for monitoring changes in the drought severity of different regions, especially against the backdrop of global warming.

The impact of climate warming on the drought sensitivity of GPP is more pronounced in coniferous forest, deciduous forest, meadow steppe, and alpine steppe. This is because vegetation growth in arid and semi-arid areas is mainly limited by insufficient moisture conditions or low water availability. This implies that, amidst global warming, changes in drought severity may have a greater impact on the role of vegetation as a carbon sink in these areas, which is consistent with the findings of extant research (Bai and Li, 2022). Rising temperatures lead to increased water loss via evapotranspiration, aggravating the severity of regional drought and resulting in more obvious water stress on vegetation (Li et al., 2018). The increase in the sensitivity of GPP to drought implies an increase in the intensity of drought effects on vegetation. Positive correlation was enhanced in areas with reduced water, while negative correlation was enhanced in areas with increased water, especially in the high latitudes of the northern hemisphere (Wei et al., 2023).

It is worth noting that the temperature increase did not seem to augment the drought sensitivity of GPP in the deciduous forest and sandy vegetation when SPI was used for monitoring. However, the area primarily controlled by precipitation in the deciduous forest accounted for the largest proportion (78.27%), showing that this area is affected by changes in water conditions. Therefore, the changes in drought severity caused by temperature rise have not been obvious. However, the moisture conditions in sandy vegetation areas have improved significantly (Fig. 3), and the adverse effects of rising temperature on the vegetation in this area were slowed down by improved moisture conditions. Wang et al. (2022c) noted that in the past 30 years, climate warming has led to warming and wetting trends in various areas of northern China, promoting the restoration of vegetation. Typical steppe, cropland, desert steppe, and sandy vegetation are mainly considered warming aridification areas (Fig. 4), and the sensitivity of their GPP to drought, as defined using SPEI, does not increase with climate warming (Fig. 8). Cropland and sandy vegetation GPP was more affected by temperature (Fig. 7), and only 37.68% and 24.39% of the vegetation areas were significantly dry, respectively. In high latitudes and humid areas in the northern hemisphere, the key factor limiting vegetation productivity is temperature rather than water availability (Ritter et al., 2020). So temperature warming did not increase the sensitivity of vegetation to drought in such areas. The vegetation productivity of typical steppe and desert steppe was mainly affected by precipitation, and the significant drying area of desert steppe reached 73.17%. This phenomenon may be due to the fact that vegetation productivity in being not only controlled by climatic factors is also influenced by vegetation physiology. For example, photosynthesis in the Amazon rainforest increases during the dry season (Green et al., 2020).

5.2 CED of drought on vegetation GPP

In arid and semi-arid regions, moisture condition is the main factor controlling vegetation growth and development. The lagged impact of precipitation on vegetation significantly outweighs that of temperature, causing precipitation to have a more lasting impact (Nie et al., 2021). In this study, shrub, deciduous forest, cropland, and sandy vegetation were found to be more susceptible to short-term drought accumulation effects under SPEI metric. The main drought-causing factors vary based on the duration of the phenomenon. Short-term drought is mainly caused by a decrease in soil moisture content and river discharge in the source area, and medium-term drought is closely related to reservoir water storage capacity and river discharge in the middle reaches. Meanwhile, changes in groundwater reserves are a key factor causing long-term drought (Vicente-Serrano et al., 2010b).

When compared with other vegetation types, the different types of grasslands in the Mongolian Plateau have longer average CED. This finding is consistent with previous studies indicating that grasslands in arid areas can adapt to long-term and high-intensity drought (Deng et al., 2020). Additionally, the difference in vegetation's root depth and biomass mostly explains the difference in CED. For example, grasslands primarily consist of herbaceous vegetation with shallow root systems, while forests comprise woody vegetation with a deep root system, allowing them to easily access water to maintain growth. Since it is generally known that CED of grassland is shorter than that of forest, the carbon sink of forest is more stable during droughts (Wolf et al., 2013; Sun et al., 2015). However, this study's results show that the cumulative effect of drought on grasslands, as characterized by SPEI, is longer than in the case of deciduous forest, which means that the drought tolerance of the plateau's grassland is higher than its deciduous forest. This may be because these herbaceous plants grow in arid and semi-arid dry climates for a long time and are exposed to prolonged soil water stress. Vegetation can reduce water loss and improve water absorption capacity by changing its growth mechanism, thus enhancing its tolerance to long-term drought (Reddy et al., 2004). Additionally, the sensitivity of grasslands located on the desert periphery to changes in drought severity may not be higher than expected (Zhang et al., 2022c).

5.3 Vegetation GPP in response to drought at different altitudes

Generally, as altitude increases, vegetation growth is influenced by a twofold dynamic: decreasing temperatures limit vegetation productivity while increasing precipitation promotes it (Piao et al., 2006; Du et al., 2019). Therefore, this study further explored the influence of drought on vegetation GPP in the Mongolian Plateau at different altitudes. It is evident that at an altitude lower than 3500 m, the sensitivity of GPP to drought, when monitored using SPI and SPEI, decreased with an increase in altitude (Fig. S1a and b). These results highlight that the drought sensitivity of GPP is closely related to the long-term climatic conditions associated with regional vertical zonality. CED related to SPI decreased at first and then increased with altitude. At 500–1000 m, the average CED was found to be the shortest (5.24 months), while the longest CED of 8.07 months was observed at an altitude higher than 3500 m. Overall, the cumulative effect of drought on GPP, as measured by SPEI, showed an upward trend, tending to stabilize at altitudes higher than 2000 m (Fig. S1c and d). This trend aligns with the findings of Zhang et al. (2022c), who noted that the cumulative effect of global drought and the drought tolerance of vegetation improved with an increase in altitude.

Previous studies have reported that in 31.81% of drought-stricken vegetation-covered areas of the world, vegetation productivity is mainly affected by short-term drought (1.00–4.00 months) (Wu and Wang, 2022). The influence of drought accumulation time on vegetation in this study area was found to last much longer than the global average drought accumulation time, an observation that can be attributed to the longer CED of grassland at middle and high latitudes. For example, after an extended cold and dry period in northern Mongolia, which typically covers the land in ice and snow, the soil moisture in spring is mainly derived from the melting snow and thawing frozen soil, promoting the growth of grasslands (Nandintsetseg and Shinoda, 2011). It is

worth noting that different GPP estimation models may yield different vegetation photosynthesis simulations due to differences in their theoretical bases (Zhang et al., 2017; Wang et al., 2021a). To understand the response relationship between vegetation and drought in a more comprehensive and in-depth manner, it is necessary to compare and explore the phenomenon from multiple perspectives.

5.4 Limitations and implications for future research

A limitation of this study is that the Mongolian Plateau is dominated by agriculture and animal husbandry economy. Consequently, GPP is not only affected by climatic factors but also by human activities and other environmental factors, especially the persistent issue of overgrazing in Mongolia and central Inner Mongolia (Guo et al., 2021). Therefore, these factors should be taken into account in future studies. The data compiled in this study simulate the inter-annual variation of GPP and drought indices on a one-month scale, so studies of differences in vegetation GPP and dry and wet conditions in different months scales of a year could be added in future work. Additionally, due to limitations in the model's structure and parameter setting, this study was unable to consider a simulation of the relationship between the vegetation's physiological process and the environment; hence, the estimation accuracy of GPP could be further improved. Few studies in the extant literature focus on the variation of drought sensitivity with altitude, particularly in regions where altitudes surpass 3500 m. Therefore, future research can expand on the description on the relationship between drought and altitude presented in this study.

6 Conclusions

This study analyzed the spatiotemporal characteristics of vegetation GPP changes and examined their correlation with different drought indices in the Mongolian Plateau from 1982 to 2018, employing the long-term EC-LUE GPP and SPI and SPEI datasets. Overall, approximately 49.47% of the total vegetation-covered areas within the region showed an upward trend in GPP, mainly concentrated in northwestern and southeastern Mongolia. The future GPP changes in 84.50% area of this region appeared to be continuous and stable. Among them, the restoration of sandy vegetation can be said to be the most significant, contrasted by the continued degradation of meadow steppe and deciduous forest. Warming aridification areas accounted for 71.40% of the Mongolian Plateau. Severe warming aridification areas accounted for 28.53% of the region, mainly in the central and southern areas of the plateau. Around 54.15% of the desert steppe belonged to the warming aridification areas. The study confirms that climate warming has increased the drought sensitivity of GPP in coniferous forest, deciduous forest, meadow steppe, and alpine steppe. In addition, the plateau's vegetation demonstrated high adaptability to long-term drought, and the average CED for the whole region was around 6.00 months. It is noteworthy that under long-term water stress, CED, as monitored using SPEI, was generally higher for grassland than for deciduous forest. The drought sensitivity of GPP decreased with an increase in altitude. The average CED of GPP to SPI first decreased and then increased with altitude. The average CED per SPEI showed an upward trend at first and then stabilized.

Conflict of interest

The authors declare that they have no known competing financial interests or personal relationships that could have appeared to influence the work reported in this paper.

Acknowledgments

This work was jointly supported by the National Natural Science Foundation of China (42361024, 42101030, 42261079, and 41961058), the Talent Project of Science and Technology in Inner Mongolia of China (NJYT22027 and NJYT23019), and the Fundamental Research Funds for the Inner Mongolia Normal University, China (2022JBBJ014 and 2022JBQN093).

Author contributions

Conceptualization: ZHAO Xuqin, LUO Min; Data curation: ZHAO Xuqin, LUO Min; Methodology: LUO Min; Investigation: MENG Fanhao, SA Chula, BAO Shanhu; Formal analysis: ZHAO Xuqin; Writing - original draft preparation: ZHAO Xuqin; Writing - review and editing: LUO Min; Funding acquisition: LUO Min, MENG Fanhao, BAO Shanhu; Resources: LUO Min, MENG Fanhao, BAO Shanhu; Supervision: LUO Min; Project administration: LUO Min; Software: LUO Min, ZHAO Xuqin; Validation: MENG Fanhao, BAO Yuhai; Visualization: ZHAO Xuqin, LUO Min, SA Chula. All authors approved the manuscript.

References

Abramopoulos F, Rosenzweig C, Choudhury B. 1988. Improved ground hydrology calculations for global climate models (GCMs): Soil water movement and evapotranspiration. Journal of Climate, 1(9): 921–941.

Agarwal S, Suchithra A S, Singh S P. 2021. Analysis and interpretation of rainfall trend using Mann-Kendall's and Sen's slope method. Indian Journal of Ecology, 48(2): 453–457.

Akhalkatsi M. 2017. Climate global change on reproduction and diversity of agricultural plants in semi-arid regions of Georgia (Caucasus Ecoregion). Agricultural Research & Technology: Open Access Journal, 3(4): 555619, doi: 10.19080/artoaj.2017.03.555619.

Bai Y, Li S G. 2022. Growth peak of vegetation and its response to drought on the Mongolian Plateau. Ecological Indicators, 141: 109150, doi: 10.1016/j.ecolind.2022.109150.

Bo Y, Li X K, Liu K, et al. 2022. Three decades of gross primary production (GPP) in China: Variations, trends, attributions, and prediction inferred from multiple datasets and time series modeling. Remote Sensing, 14(11): 2564, doi: 10.3390/rs14112564.

Charlton C, Stephenson T, Taylor M A, et al. 2022. Evaluating skill of the Keetch–Byram drought index, vapour pressure deficit and water potential for determining bushfire potential in Jamaica. Atmosphere, 13(8): 1276, doi: 10.3390/atmos13081267.

Chen S L, Huang Y F, Wang G Q. 2021. Detecting drought-induced GPP spatiotemporal variabilities with sun-induced chlorophyll fluorescence during the 2009/2010 droughts in China. Ecological Indicators, 121: 107092, doi: 10.1016/j.ecolind.2020.107092.

Chen X N, Tao X, Yang Y P. 2022. Distribution and attribution of gross primary productivity increase over the Mongolian Plateau, 2001–2018. IEEE Access, 10: 25125–25134.

Chu D, Shen H F, Guan X B, et al. 2021. Long time-series NDVI reconstruction in cloud-prone regions via spatio-temporal tensor completion. Remote Sensing of Environment, 264: 112632, doi: 10.1016/j.rse.2021.112632.

Cui T X, Wang Y J, Sun R, et al. 2017. Estimating vegetation primary production in the Heihe river basin of China with multi-source and multi-scale data. PLoS ONE, 11(4): e0153971, doi: 10.1371/journal.pone.0153971.

Dannenberg M P, Yan D, Barnes M L, et al. 2022. Exceptional heat and atmospheric dryness amplified losses of primary production during the 2020 U.S. Southwest hot drought. Global Change Biology, 28(16): 4794–4806.

Deng H Y, Yin Y H, Han X. 2020. Vulnerability of vegetation activities to drought in Central Asia. Environmental Research Letters, 15(8): 084005, doi: 10.1088/1748-9326/ab93fa.

Du J, He Z B, Piatek B K, et al. 2019. Interacting effects of temperature and precipitation on climatic sensitivity of spring vegetation green-up in arid mountains of China. Agricultural and Forest Meteorology, 269–270: 71–77.

Feng S, Fu Q. 2013. Expansion of global drylands under a warming climate. Atmospheric Chemistry and Physics, 13(19): 10081–10094.

Green J K, Berry J, Ciais P, et al. 2020. Amazon rainforest photosynthesis increases in response to atmospheric dryness. Science Advances, 6(47): eabb7232, doi: 10.1126/sciadv.abb7232.

Gu X L, Guo E L, Yin S, et al. 2022. Differentiating cumulative and lagged effects of drought on vegetation growth over the Mongolian Plateau. Ecosphere, 13(12): e4289, doi: 10.1002/ecs2.4289.

Guan X B, Chen J M, Shen H F, et al. 2022. Comparison of big-leaf and two-leaf light use efficiency models for GPP simulation after considering a radiation scalar. Agricultural and Forest Meteorology, 313: 108761, doi: 10.1016/j.agrformet.2021.108761.

Guo E L, Wang Y F, Wang C L, et al. 2021. NDVI indicates long-term dynamics of vegetation and its driving forces from climatic and anthropogenic factors in Mongolian Plateau. Remote Sensing, 13(4): 688, doi: 10.3390/rs13040688.

Hang J, Guan X, Ji F. 2012. Enhanced cold-season warming in semi-arid regions. Atmospheric Chemistry and Physics, 12(12): 5391–5398.

Hayes M, Svoboda M, Wall N, et al. 2011. The Lincoln Declaration on drought indices: Universal meteorological drought index

recommended. Bulletin of the American Meteorological Society, 92(4): 485–488.

He B, Tuya W, Qinchaoketu S, et al. 2022a. Climate change characteristics of typical grassland in the Mongolian Plateau from 1978 to 2020. Sustainability, 14(24): 16529, doi: 10.3390/su142416529.

He P X, Ma X L, Meng X Y, et al. 2022b. Spatiotemporal evolutionary and mechanism analysis of grassland GPP in China. Ecological Indicators, 143: 109323, doi: 10.1016/j.ecolind.2022.109323.

Huang Y C, Liu B W, Zhao H G, et al. 2022. Spatial and temporal variation of droughts in the Mongolian Plateau during 1959–2018 based on the gridded self-calibrating palmer drought severity index. Water, 14(2): 230, doi: 10.3390/w14020230.

Ji J Y, Lin H. 2022. Evaluating regional carbon inequality and its dependence with carbon efficiency: implications for carbon neutrality. Energies, 15(19): 7022, doi: 10.3390/en15197022.

Jiang C Y, Ryu Y. 2016. Multi-scale evaluation of global gross primary productivity and evapotranspiration products derived from Breathing Earth System Simulator (BESS). Remote Sensing of Environment, 186: 528–547.

Kang Y, Guo E L, Wang Y F, et al. 2021. Application of temperature vegetation dryness index for drought monitoring in Mongolian Plateau. Chinese Journal of Applied Ecology, 32(7): 2534–2544.

Kocsis T, Kovács-Székely I, Anda A. 2020. Homogeneity tests and non-parametric analyses of tendencies in precipitation time series in Keszthely, Western Hungary. Theoretical and Applied Climatology, 139(3): 849–859.

Li C L, Filho L W, Yin J, et al. 2018. Assessing vegetation response to multi-time-scale drought across Inner Mongolia Plateau. Journal of Cleaner Production, 179: 210–216.

Li G S, Yu L X, Liu T X, et al. 2023. Spatial and temporal variations of grassland vegetation on the Mongolian Plateau and its response to climate change. Frontiers in Ecology and Evolution, 11: 1067209, doi: 10.3389/fevo.2023.1067209.

Li S J, Wang J M, Zhang M, et al. 2021. Characterizing and attributing the vegetation coverage changes in North Shanxi coal base of China from 1987 to 2020. Resources Policy, 74: 102331, doi: 10.1016/j.resourpol.2021.102331.

Luo M, Meng F H, Sa C L, et al. 2021. Response of vegetation phenology to soil moisture dynamics in the Mongolian Plateau. Catena, 206: 105505, doi: 10.1016/j.catena.2021.105505.

McKee T B, Doesken N J, Kleist J. 1993. The relationship of drought frequency and duration to time scales. Eighth Conference on Applied Climatology, 17–22.

Meng F H, Luo M, Wang Y Q, et al. 2023. Revisiting the main driving factors influencing the dynamics of gross primary productivity in the Mongolian Plateau. Agricultural and Forest Meteorology, 341: 109689, doi: 10.1016/j.agrformet.2023.109689.

Na R S, Na L, Du H B, et al. 2021. Vegetation greenness variations and response to climate change in the arid and semi-arid transition zone of the Mongo-Lian Plateau during 1982–2015. Remote Sensing, 13(20): 4066, doi: 10.3390/rs13204066.

Nandintsetseg B, Shinoda M. 2011. Seasonal change of soil moisture in Mongolia: its climatology and modelling. International Journal of Climatology, 31(8): 1143–1152.

Neda K, Hossein R, Javad B. 2022. Investigation of drought trend on the basis of the best obtained drought index. Water Resources Management, 36(4): 1355–1375.

Nie T, Dong G T, Jiang X H, et al. 2021. Spatio-temporal changes and driving forces of vegetation coverage on the loess Plateau of Northern Shaanxi. Remote Sensing, 13(4): 613, doi: 10.3390/rs13040613.

Pan L, Xia H M, Zhao X Y, et al. 2021. Mapping winter crops using a phenology algorithm, time-series sentinel-2 and landsat-7/8 images, and google earth engine. Remote Sensing, 13(13): 2510, doi: 10.3390/ rs13132510.

Pei Y Y, Dong J W, Zhang Y, et al. 2022. Evolution of light use efficiency models: improvement, uncertainties, and implications. Agricultural and Forest Meteorology, 317: 108905, doi: 10.1016/j.agrformet.2022.108905.

Peng J, Wu C Y, Wang X Y, et al. 2019. Satellite detection of cumulative and lagged effects of drought on autumn leaf senescence over the Northern Hemisphere. Global Change Biology, 25(6): 2174–2188.

Piao S L, Amwar M, Fang J Y, et al. 2006. NDVI-based increase in growth of temperate grasslands and its responses to climate changes in China. Global Environmental Change, 16(4): 340–348.

Piao S L, Sitch S, Ciais P, et al. 2013. Evaluation of terrestrial carbon cycle models for their response to climate variability and to CO_2 trends. Global Change Biology, 19(7): 2117–2132.

Piao S L, He Y, Wang X H, et al. 2022. Estimation of China's terrestrial ecosystem carbon sink: methods, progress and prospects. Science China (Earth Sciences), 65(4): 641–651.

Qu S, Wang L C, Lin A W, et al. 2020. Distinguishing the impacts of climate change and anthropogenic factors on vegetation dynamics in the Yangtze River Basin, China. Ecological Indicators, 108: 105724, doi: 10.1016/j.ecolind.2019.105724.

Reddy A R, Chaitanya K V, Vivekanandan M. 2004. Drought-induced responses of photosynthesis and antioxidant metabolism in higher plants. Journal of Plant Physiology, 161(11): 1189–1202.

Ritter F, Berkelhammer M, Garcia-Eidell C. 2020. Distinct response of gross primary productivity in five terrestrial biomes to

precipitation variability. Communications Earth & Environment, 1(1): 34, doi: 10.1038/s43247-020-00034-1.

Sun S L, Sun G, Peter C, et al. 2015. Drought impacts on ecosystem functions of the U.S. National Forests and Grasslands: Part II assessment results and management implications. Forest Ecology and Management, 353: 269–279.

Vanikiotis T, Stagakis S, Kyparissis A. 2021. MODIS PRI performance to track light use efficiency of a Mediterranean coniferous forest: Determinants, restrictions and the role of LUE range. Agricultural and Forest Meteorology, 307: 108518, doi: 10.1016/j.agrformet.2021.108518.

Vicente-Serrano S M, Beguería S, López-Moreno J. 2010a. A multiscalar drought index sensitive to global warming: The standardized precipitation evapotranspiration index. Journal of Climate, 23(7): 1696–1718.

Vicente-Serrano S M, Beguería S, López-Moreno J, et al. 2010b. A new global 0.5° gridded dataset (1901–2006) of a multiscale drought index: Comparison with current drought index datasets based on the Palmer drought severity index. Journal of Hydrometeorology, 11(4): 1033–1043.

Wang K, Bastos A, Ciais P, et al. 2022a. Regional and seasonal partitioning of water and temperature controls on global land carbon uptake variability. Nature Communications, 13(1): 3469, doi: 10.1038/s41467-022-31175-w.

Wang M J, Sun R, Zhu A R, et al. 2020. Evaluation and comparison of light use efficiency and gross primary productivity using three different approaches. Remote Sensing, 12(6): 1003, doi: 10.3390/rs12061003.

Wang M M, Wang S Q, Wang J B, et al. 2018. Detection of positive gross primary production extremes in terrestrial ecosystems of China during 1982–2015 and analysis of climate contribution. Journal of Geophysical Research: Biogeosciences, 123(9): 2807–2823.

Wang S H, Zhang Y G, Ju W M, et al. 2021a. Tracking the seasonal and inter-annual variations of global gross primary production during last four decades using satellite near-infrared reflectance data. Science of the Total Environment, 755(P2): 142569, doi: 10.1016/j.scitotenv.2020.142569.

Wang S P, Wang J S, Zhang Q, et al. 2016. Cumulative effect of precipitation deficit preceding severe droughts in southwestern and southern China. Discrete Dynamics in Nature and Society, 2016: 2890852, doi: 10.1155/2016/2890852.

Wang Y H, Fu Z, Hu Z M, et al. 2022b. Tracking global patterns of drought-induced productivity loss along severity gradient. Journal of Geophysical Research: Biogeosciences, 127(6): e2021JG006753, doi: 10.1029/2021jg006753.

Wang Z, Liu S G, Wang Y P, et al. 2021b. Tighten the bolts and nuts on GPP estimations from sites to the globe: An assessment of remote sensing based LUE models and supporting data fields. Remote Sensing, 13(2): 168, doi: 10.3390/rs13020168.

Wang Z, Zhang T L, Pei C Y, et al. 2022c. Multisource remote sensing monitoring and analysis of the driving forces of vegetation restoration in the Mu Us sandy land. Land, 11(9): 1553, doi: 10.3390/land11091553.

Wei X N, He W, Zhou Y L, et al. 2022. Global assessment of lagged and cumulative effects of drought on grassland gross primary production. Ecological Indicators, 136: 108646, doi: 10.1016/j.ecolind.2022.108646.

Wei X N, He W, Zhou Y L, et al. 2023. Increased sensitivity of global vegetation productivity to drought over the recent three decades. Journal of Geophysical Research: Atmospheres, 128(7): e2022JD037504, doi: 10.1029/2022JD037504.

Wolf S, Eugster W, Ammann C, et al. 2013. Contrasting response of grassland versus forest carbon and water fluxes to spring drought in Switzerland. Environmental Research Letters, 8(3): 035007, doi: 10.1088/1748-9326/8/3/035007.

Wu C L, Wang T J. 2022. Evaluating cumulative drought effect on global vegetation photosynthesis using numerous GPP products. Frontiers in Environmental Science, 10: 908875, doi: 10.3389/fenvs.2022.908875.

Wu X P, Zhang R R, Bento V A, et al. 2022. The effect of drought on vegetation gross primary productivity under different vegetation types across China from 2001 to 2020. Remote Sensing, 14(18): 4658, doi: 10.3390/rs14184658.

Xiao J F, Chevallier F, Gomez C, et al. 2019. Remote sensing of the terrestrial carbon cycle: A review of advances over 50 years. Remote Sensing of Environment, 233: 111383, doi: 10.1016/j.rse.2019.111383.

Xie X Y, Li A N. 2020. Development of a topographic-corrected temperature and greenness model (TG) for improving GPP estimation over mountainous areas. Agricultural and Forest Meteorology, 295: 108193, doi: 10.1016/j.agrformet.2020.108193.

Xie Z Y, Zhao C L, Zhu W Q, et al. 2023. A radiation-regulated dynamic maximum light use efficiency for improving gross primary productivity estimation. Remote Sensing, 15(5): 1176, doi: 10.3390/rs15051176.

Xiong Q, Sun Z Y, Cui W, et al. 2022. A study on sensitivities of tropical forest GPP responding to the characteristics of drought—A case study in Xishuangbanna, China. Water, 14(2): 157, doi: 10.3390/w14020157.

Xu H L, Chen Y N, Li W H. 2003. Multiple regression analysis of the relationship between environmental factors and desertification in the lower Tarim River. Arid Zone Research, 20(1): 39–43. (in Chinese)

Yin C H, Luo M, Meng F H, et al. 2022. Contributions of climatic and anthropogenic drivers to net primary productivity of vegetation in the Mongolian Plateau. Remote Sensing, 14(14): 3383, doi: 10.3390/rs14143383.

Yin C H, Chen X Q, Luo M, et al. 2023. Quantifying the contribution of driving factors on distribution and change of net

primary productivity of vegetation in the Mongolian Plateau. Remote Sensing, 15(8): 1986, doi: 10.3390/rs15081986.

Yu T, Sun R, Xiao Z Q, et al. 2018. Estimation of global vegetation productivity from global land surface satellite data. Remote Sensing, 10(2): 327, doi: 10.3390/rs10020327.

Yuan W P, Liu S G, Yu G R, et al. 2010. Global estimates of evapotranspiration and gross primary production based on MODIS and global meteorology data. Remote Sensing of Environment, 114(7): 1416–1431.

Zhan C, Liang C, Zhao L, et al. 2022. Drought-related cumulative and time-lag effects on vegetation dynamics across the Yellow River Basin, China. Ecological Indicators, 143: 109409, doi: 10.1016/j.ecolind.2022.109409.

Zhang B Q, Wu P T, Zhao X N, et al. 2012. Changes in vegetation condition in areas with different gradients (1980–2010) on the Loess Plateau, China. Environmental Earth Sciences, 68(8): 2427–2438.

Zhang M, Yuan X, Otkin J A. 2020. Remote sensing of the impact of flash drought events on terrestrial carbon dynamics over China. Carbon Balance and Management, 15(1): 20, doi: 10.1186/s13021-020-00156-1.

Zhang S Z, Zhu X F, Liu T T, et al. 2022a. Response of gross primary production to drought under climate change in different vegetation regions of China. Acta Ecologica Sinica, 42(8): 3429–3440. (in Chinese)

Zhang X, Sa C L, Hai Q S, et al. 2023. Quantifying the effects of snow on the beginning of vegetation growth in the Mongolian Plateau. Remote Sensing, 15(5): 1245, doi: 10.3390/rs15051245.

Zhang Y, Xiao X M, Wu X C, et al. 2017. A global moderate resolution dataset of gross primary production of vegetation for 2000–2016. Scientific Data, 4(1): 170165, doi: 10.1038/sdata.2017.165.

Zhang Y Z, Wang Z Q, Wang Q, et al. 2022b. Comparative assessment of grassland dynamic and its response to drought based on multi-index in the Mongolian Plateau. Plants, 11(3): 310, doi: 10.3390/plants11030310.

Zhang Z Y, Ju W M, Zhou Y L, et al. 2022c. Revisiting the cumulative effects of drought on global gross primary productivity based on new long-term series data (1982–2018). Global Change Biology, 28(11): 3620–3635.

Zhao X, Ma X W, Chen B Y, et al. 2022. Challenges toward carbon neutrality in China: Strategies and countermeasures. Resources, Conservation & Recycling, 176: 105959, doi: 10.1016/J.RESCONREC.2021.105959.

Zhen Z, Flurin B, Valentin B, et al. 2018. Converging climate sensitivities of European forests between observed radial tree growth and vegetation models. Ecosystems, 21(3): 410–425.

Zheng Y, Shen R Q, Wang Y W, et al. 2020. Improved estimate of global gross primary production for reproducing its long-term variation, 1982–2017. Earth System Science Data, 12(4): 2725–2746.

Appendix

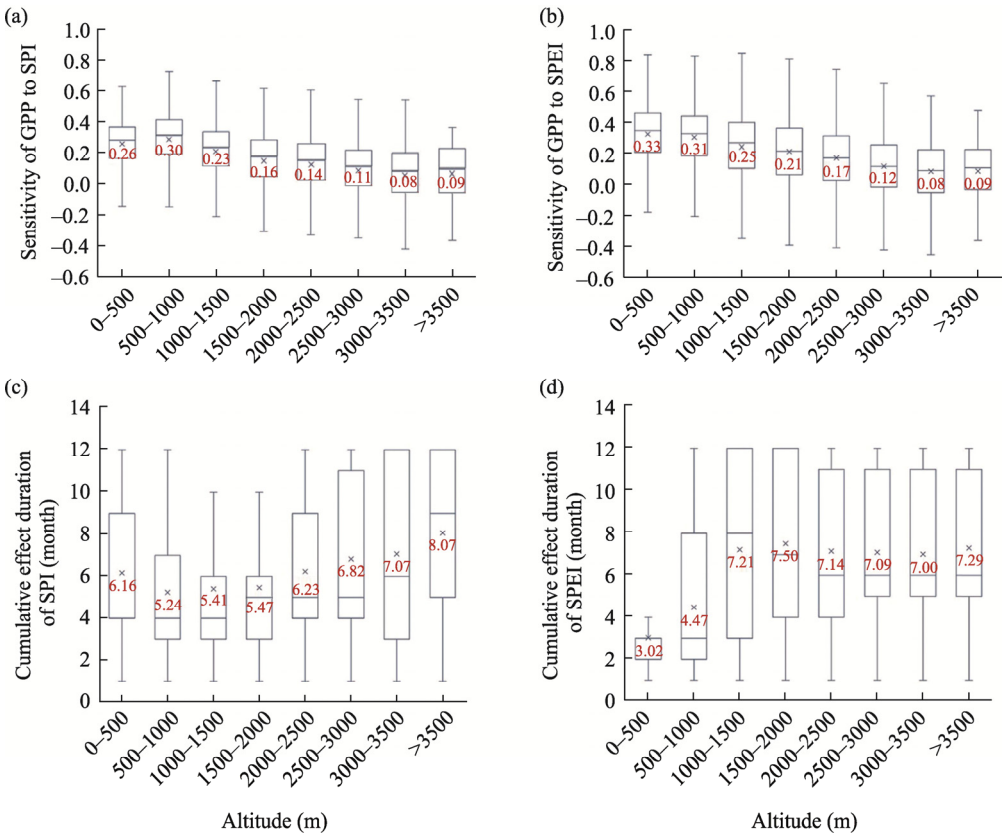

Fig. S1 Altitude dependence of gross primary productivity (GPP) on drought sensitivity and drought accumulation. SPI, standardized precipitation index; SPEI, standardized precipitation evapotranspiration index. The boxes represent the range from the lower quantile (Q25) to the upper quantile (Q75). The cross symbols and horizontal lines inside the boxes represent the means and medians, respectively. The upper and lower whiskers indicate the maximum and minimum values, respectively.